Transparent, Stimuli-Responsive Films from Cellulose-Based Organogel Nanoparticles

*Yonggui Wang, Lars-Oliver Heim, Yeping Xu, Gerd Buntkowsky, and Kai Zhang**

The use of bio-based nanoscaled cellulose for the construction of novel functional materials has progressed rapidly over the past years. In comparison to most of studies starting with the hydrophilic nanoscaled cellulose, surface-stearoylated cellulose nanoparticles (SS-CNPs) are used in this report for the construction of multifunctional, responsive films. SS-CNPs with an average size of 115 ± 0.5 nm are obtained after the surface-modification of cellulose under heterogeneous conditions. Crystalline cellulose core is present within SS-CNPs according to solid-state ^{13}C nuclear magnetic resonance (NMR) spectroscopy. SS-CNPs show excellent dispersibility in nonpolar solvents and form temperature-responsive organogels in tetrahydrofuran (THF) at low temperature or after long time storage at room temperature. Moreover, transparent and self-standing films of SS-CNPs from their THF-suspension show solvent-responsive surface wettability and responsive shape-memory property. SS-CNPs can also be used for the fabrication of nanocomposite films together with nonpolar compounds, such as (2-stearoylaminoethyl) rhodamine B. Thus, these novel SS-CNPs derived from sustainable cellulose fibers are promising candidates for the construction of novel functional materials.

1. Introduction

Nanocellulose-based materials received increasing attentions, not only due to the sustainable nature of cellulose, but also due to its advantageous properties, such as excellent biocompatibility, nontoxicity and biodegradability.[1] In particular, nanocellulose and functionalized nanocellulose are excellent reinforcing component for the construction of diverse shapes of materials, such as films, fibers or aerogels.[1a,2] Films from nanocellulose are generally translucent and flexible, but strongly hydrophilic.[3] In order to improve the properties of films from nanocellulose, other matrix materials such as hydrophobic synthetic polymers are often used with nanocellulose as reinforcing nanofiller.[4] However, the dispersibility of nanocellulose within the matrix and its interfacial interaction with other matrix components play a pivotal role for the final properties of the obtained materials, such as mechanical performance.[5] In particular, the poor dispersibility of nanocellulose in nonpolar solvents and weak interactions with nonpolar synthetic polymers are the main drawbacks limiting the full performance of nanocellulose. In order to improve these issues, nanocellulose is generally surface-modified with functional groups, such as alkyl groups or synthetic polymers via "grafting to" as well as "grafting from" techniques.[6]

In particular, surface-modified nanocellulose by alkyl chains is supposed to be well miscible with other synthetic polymers and exist as reinforcing nanofillers in diverse materials, including films and foams.[1b,6a,d,7] Several different methods have been used for the immobilization of alkyl groups on nanocellulose surface. Generally, a postmodification of hydroxyl- or carboxyl groups on nanocellulose surface is preferred. Cellulose nanocrystals (CNC) were modified by palmitoyl chloride vapor during a gas-phase esterification process or surface-modified by acid chloride.[8] The palmitated cellulose nanocrystals showed the feasibility to form gels in toluene.[9] In addition, nanocellulose showing similar properties could also be synthesized after the modification using *n*-octadecyl isocyanate,[10] isocyanate-terminated castor oil,[11] or octadecylamine.[6a,7b] They formed films after casting, which exhibited limited hydrophobicity with static water contact angles of up to 100°, but good water vapor and oxygen barrier feasibility. Thus, a chemical postmodification of water-borne CNC has to be performed, in order to endow films from CNC particular functions.

Herein, we report the fabrication of multifunctional, self-standing films using surface-stearoylated cellulose organogel nanoparticles (SS-CNPs) showing stimuli-responsive properties. SS-CNPs were obtained via a novel synthesis route after a one-step esterification of cellulose fibers under heterogeneous

Y. Wang, Dr. K. Zhang
Ernst-Berl-Institute for Chemical Engineering and Macromolecular Science
Technische Universität Darmstadt
Alarich-Weiss-Str. 8, D-64287 Darmstadt, Germany
E-mail: zhang@cellulose.tu-darmstadt.de
Dr. L.-O. Heim
Center of Smart Interfaces
Technische Universität Darmstadt
Alarich-Weiss-Straße 10, D-64287 Darmstadt, Germany
Dr. Y. Xu, Prof. G. Buntkowsky
Eduard-Zintl-Institute for Inorganic Chemistry and Physical Chemistry
Technische Universität Darmstadt
Alarich-Weiss-Straße 4
D-64287 Darmstadt, Germany

DOI: 10.1002/adfm.201403067

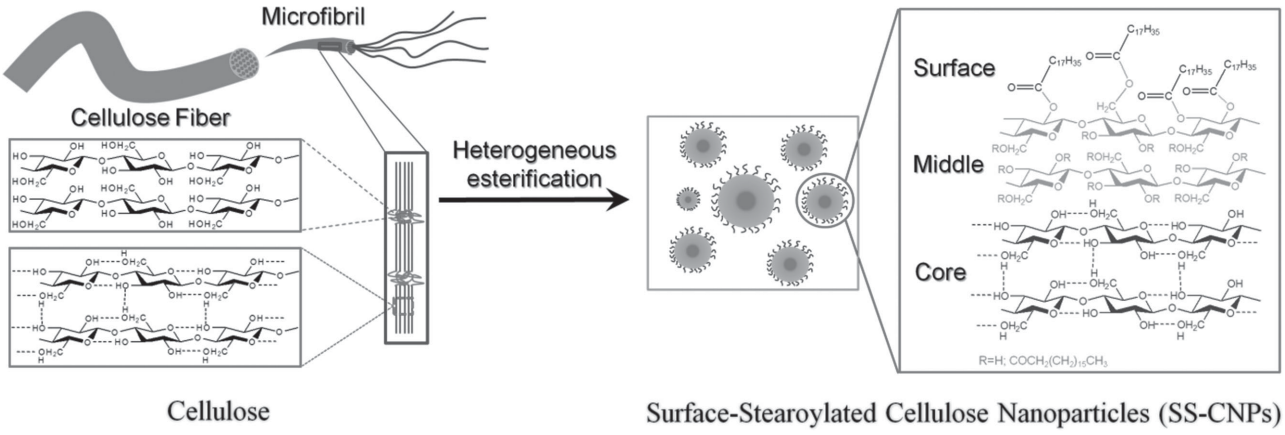

Scheme 1. Schematic illustration for the fabrication of SS-CNPs from cellulose.

reaction conditions using stearoyl chloride and a follow-up purification process. The chemical structure, crystalline structure, and morphology of obtained SS-CNPs were elucidated using elemental analysis, Fourier transform infrared spectroscopy (FTIR spectroscopy), solid-state ^{13}C NMR spectroscopy, dynamic light scattering (DLS), and scanning electron microscopy (SEM). The thermo-reversible gelation behavior of SS-CNPs in tetrahydrofuran (THF) was studied by rheological measurements. SS-CNPs were further used to fabricate self-standing, transparent and hydrophobic films, which were characterized regarding their morphology, solvent-responsive surface wettability and responsive shape-memory property. Moreover, a nanocomposite film of SS-CNPs and (2-stearoylaminoethyl) rhodamine B (C_{18}–RhB) with UV- and temperature-responsiveness, and reversible fluorescence was successfully constructed.

2. Results and Discussion

2.1. Surface-Stearoylated Cellulose Nanopartilces (SS-CNPs)

SS-CNPs were obtained after the surface esterification of cellulose by stearoyl chloride under heterogeneous conditions (**Scheme 1**). The degree of substitution (DS) of SS-CNPs was determined to be 1.33 based on the elemental analysis.[12] FTIR spectrum of SS-CNPs shows characteristic bands ascribed to both cellulose backbone and stearoyl groups (**Figure 1**a). Typical FTIR bands of cellulose are visible, such as the bands attributed to vibrations of O–H (3000–3600 and 1300–1450 cm^{-1}), C–H (2900 cm^{-1}), and C–O groups (950–1200 cm^{-1}).[9b] The successful stearoylation is characterized by the significant increase of bands at 2910, 2840, 1466, 1164, and 720 cm^{-1}, which are attributed to asymmetric C–H stretching vibrations, symmetric C–H stretching vibrations, symmetric C–H deformation vibrations, C–O–C stretching vibrations and C–C rocking vibrations, respectively.[13] A new band appears at 1746 cm^{-1}, which is derived from C=O stretching vibrations of ester bonds.[13a] Solid-state ^{13}C NMR spectrum of starting microcrystalline cellulose (MCC) exhibited a typical pattern with an intense signal of C1 (105.5 ppm) and a signal as doublet of C4 (85.5 ppm) (Figure 1b), which is characteristic for highly crystalline cellulose I.[14] The solid-state ^{13}C NMR spectrum of SS-CNPs showed the peak at 173 ppm ascribed to the carbon from the ester linkage and the signals between 40 and 10 ppm due to the carbons within the aliphatic groups.[15] Moreover, the signal at ≈88.5 ppm attributed to crystalline cellulose is still visible. Hence, a crystalline cellulose core is still maintained in SS-CNPs.

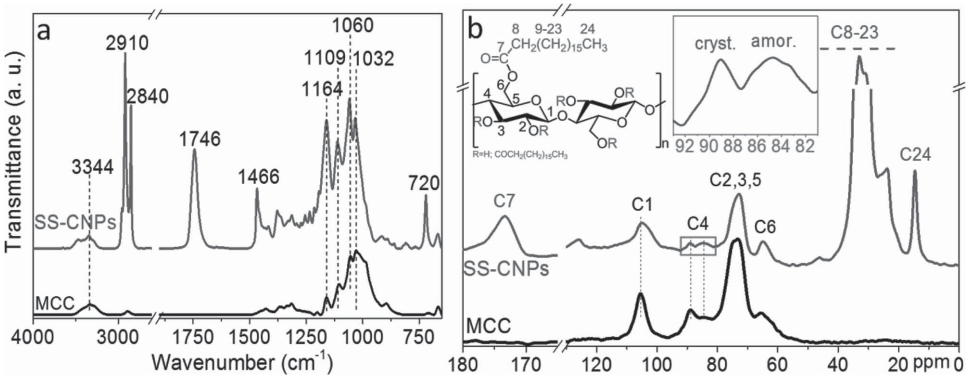

Figure 1. a) FTIR spectra of MCC and SS-CNPs; b) Solid-state CP/MAS ^{13}C NMR spectra of MCC and SS-CNPs. The inset shows the chemical structure of substituted anhydroglucose units of cellulose and the enlarged NMR region of 93–81 ppm.

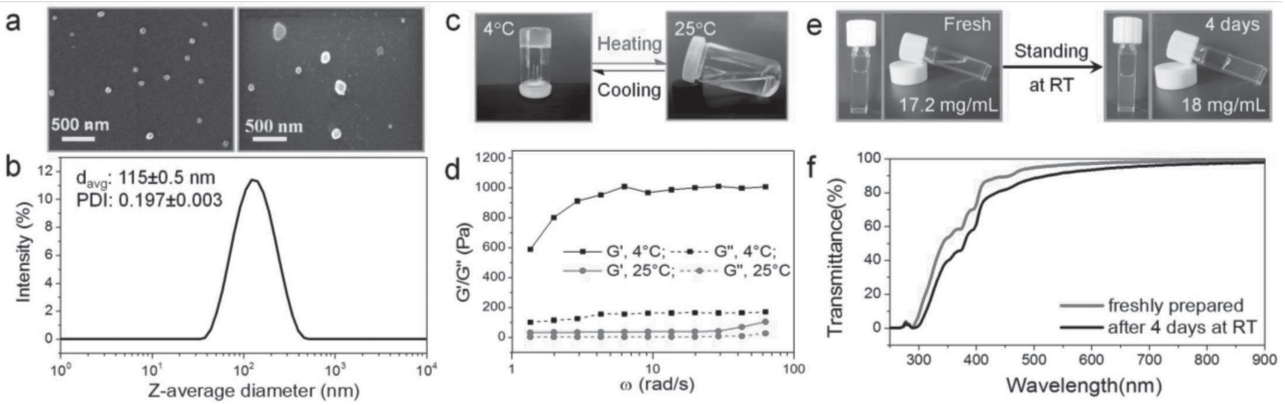

Figure 2. a) Representative SEM images of SS-CNPs; b) Size distribution of SS-CNPs in THF based on DLS measurement at 25 °C; c) Photo images of SS-CNPs suspension in THF (20 mg mL^{-1}) at 4 and 25 °C; d) Elastic (G′) and viscous (G″) modulus as a function of oscillatory shear frequency of SS-CNPs in THF (20 mg mL^{-1}) at 4 and 25 °C; e) Photo images of gelation process of SS-CNPs in THF at room temperature; f) UV–vis transmittance spectra of freshly prepared THF-suspension of SS-CNPs and the same suspension after 4 d storage.

Due to the existence of crystalline cellulose, SS-CNPs cannot be dissolved by the common organic solvents, but can be well swollen by THF, dichloromethane, cyclohexane, and other non-polar organic solvents. The suspensions of SS-CNPs in different solvents were stable and (semi)transparent even after storage at room temperature (RT) for long time, e.g., 7 d (Figure S1, Supporting Information). SS-CNPs in THF have an average diameter of 115 ± 0.5 nm according to DLS measurement with a relatively high polydispersity index (PDI) of 0.197 (**Figure 2**b). As evidenced by SEM (Figure 2a), the sizes of SS-CNPs range from a few dozens to hundreds of nm, which is consistent with the DLS analysis. Furthermore, their shapes are not uniformly regularly spherical (Figures 2a, and S2, Supporting Information). The irregular shapes and the relatively high polydispersity are due to the step-wise esterification of cellulose fibers under heterogeneous reaction conditions, which generally begins from the fiber surface and then extents to the core.[9c] The multidisperse size of starting MCC is probably another reason.

The SS-CNPs suspensions exhibited a thermo-reversible gelation behavior (Figure 2c,d). When the transparent THF-suspension of SS-CNPs was stored at 4 °C for 2 h, it became a viscoelastic organogel (Figure 2c). When the temperature was increased to 25 °C, the sample regressed to the initial state. The viscoelasticity of SS-CNPs suspensions at 4 and 25 °C was evaluated via rheometry to measure the elastic (G′) and viscous (G″) modulus (Figure 2d). The rheological response of the sample at 4 °C was highly elastic, with G′ being much higher than G″ at all shear frequencies.[16] At 25 °C, the elastic (G′) and viscous (G″) modulus decreased simultaneously, but the extent of the G′ reduction was much higher than that of G″, allowing the transition from gel to sol state. Thus, a reversible gelling and de-gelling process of SS-CNPs in THF occurs in response to the temperature. During the reduction of the temperature, the swelling ability of SS-CNPs in THF decreased causing the aggregation of SS-CNPs, while the dispersibility increases with rising temperature.

Furthermore, the THF-suspension of SS-CNPs could also form organogel at RT, e.g., after the storage for 4 d (Figure 2e). The slight increase of concentration caused by the evaporation of THF during the storage is not the reason for gelation, because freshly-prepared THF-suspension of SS-CNPs with the same concentration (18 mg mL^{-1}) still maintained the sol state (Figure S3, Supporting Information). The slow equilibration under static conditions of interactions between stearoyl groups and between them and THF is probably the reason. In addition, the transparency of the suspension slightly decreased accompanying the gelation (Figure 2f).

2.2. Transparent, Self-Standing Films with Switchable Surface Wettability

Transparent and self-standing films were fabricated by solvent casting of THF-suspensions of SS-CNPs (**Figure 3**a). After the evaporation of THF, transparent films with relatively smooth surfaces (roughness 5.1 ± 2.4 nm) were obtained (Figure 3b). The films are composed of stacked layers, which are similar to the films fabricated using other nanoscaled cellulose materials, such as nanofibrillated cellulose (Figure 3c).[17] In comparison, microscaled, surface-stearoylated cellulose fibers are not feasible to fabricate such transparent and self-standing films, but only opaque rough layers (Figure S4, Supporting Information). Thus, the nanodimension of SS-CNPs is critical for the formation of transparent and self-standing films.

Furthermore, these films exhibited solvent-switchable surface wettability (Figure 3e). Freshly-prepared films exhibited a static water contact angle of about 102 ± 2°, while the contact angle increased to around 115° after treating with acetone for 10 s (Figure 3a). This increased surface-hydrophobicitiy represented by higher contact angle could be switched back via dipping in THF. Since the same films were used, the only difference between THF-treated F1-THF-n and acetone-treated F1-AT-*n* is different surface roughness. The higher roughness of F1-AT-1 compared to that of F1-THF-1 was confirmed by the atomic force microscopy (AFM) measurements (Figure 3d and 3g). Moreover, the layered structure of the films was maintained during the treatment with acetone (Figure 3c,f).

In comparison to THF, acetone is not a good dispersing medium for SS-CNPs. SS-CNPs rapidly form large aggregates after the transfer from THF into acetone. The deposition of

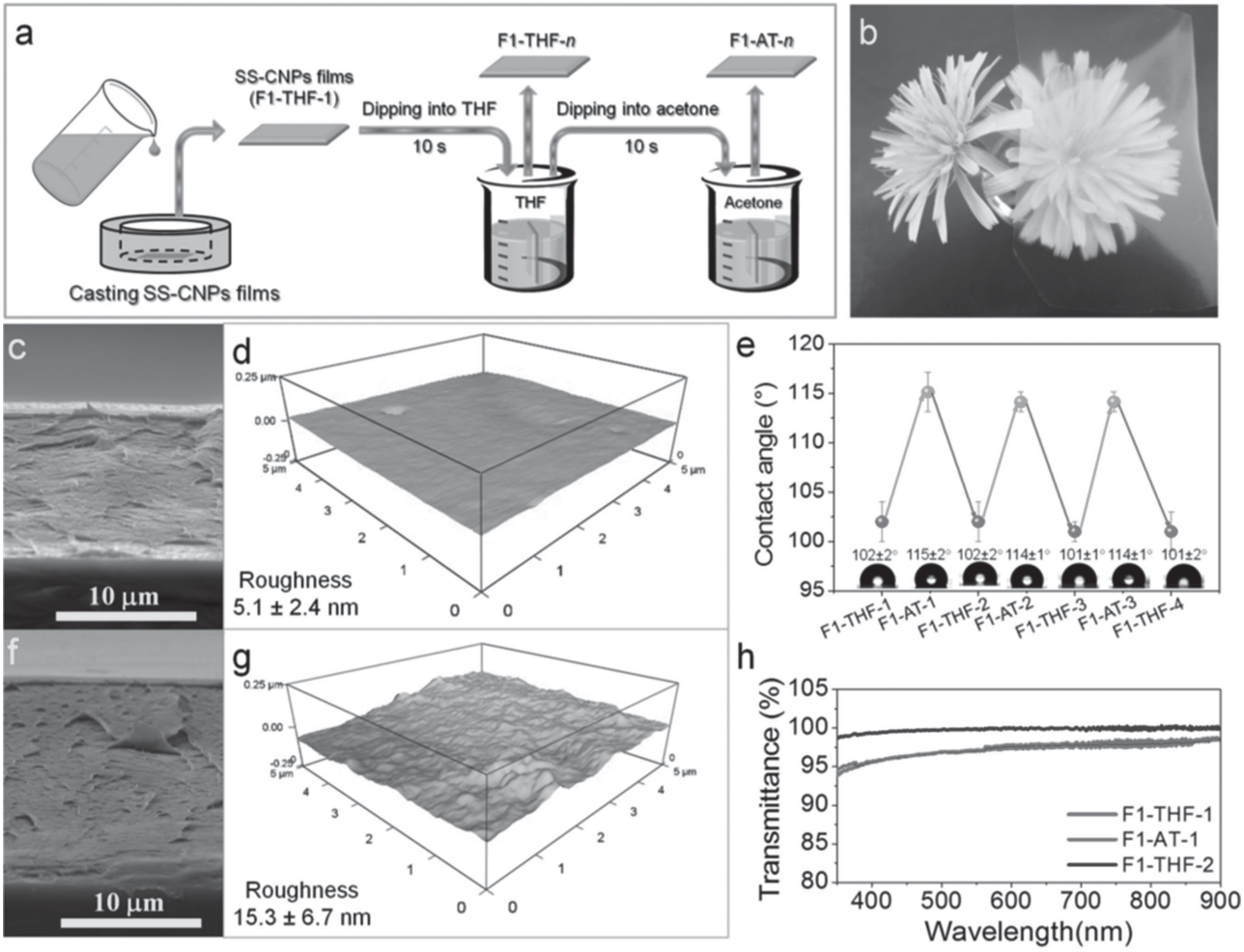

Figure 3. a) Schematic illustration for the fabrication of SS-CNPs films and further treatment demonstrating solvent-responsive surface-wettability; b) A representative photo image of SS-CNPs film; c) SEM image of the cross section and d) 3D AFM image of F1-THF-1 film; e) Static water contact angles of SS-CNPs films after alternative treatments with THF and acetone; f) SEM image of the cross section; and g) 3D AFM image of F1-AT-1 film; h) UV–vis transmittance spectra of SS-CNPs films at RT.

such aggregates of SS-CNPs in acetone resulted in nonuniform aggregation of SS-CNPs after the evaporation of acetone, leading to semi-transparent layers with solvent-switchable surface wettability (Figures S5,S6, Supporting Information). However, the layers were very brittle and could not be separated as self-standing films. In contrast, SS-CNPs dried from THF-suspension formed more homogeneous films with layered structure due to the strong interaction between stearoyl groups and THF.[15] Thus, during the reversible change of the surface roughness, THF and acetone took the role as smoothing and roughing agent, respectively. The switching of the surface roughness is totally reversible and requires only 10 s treatment using corresponding solvent (Figure 3a,e).

Hence, the SS-CNPs contains crystalline cellulose core and surface-attached stearoyl groups exhibit promising properties, including the gelation at low temperature and the formation of transparent, self-standing films. Different interactions between SS-CNPs and diverse solvents, such as THF and acetone, allowed the feasibility of reversibly modifying the surface roughness and therefore the surface wettability.

The fabrication of composite materials is a good strategy to provide multifunctions or to involve new properties that are not available using single-component materials.[18] Using the transparent SS-CNPs films, nanocomposite films containing other functional components could be readily prepared. (2-stearoylaminoethyl) rhodamine B (C_{18}–RhB) derived from rhodamine spiroamide was chosen as model compound, because rhodamine is a photostable fluorescent dye with broad applications in biomedical sensing and imaging (Scheme S1 and Figure S7, Supporting Information).[19] After the incorporation of C_{18}–RhB, SS-CNPs films were endowed with UV- and temperature-responsiveness with switchable optical color as well as fluorescence (**Figure 4**a). After the UV-illumination at 365 nm for 30 min, the color became magenta and UV–vis absorption at 560 nm strongly increased, while 1 h treatment at 135 °C resulted in color fading and weak UV–vis absorption at 560 nm (Figures 4a and S8, Supporting Information). The reversible changes of optical color and fluorescence could be repeated for several times (Figure 4a–c). After the repetitive irradiation and heating, the relative intensity of the fluorescence

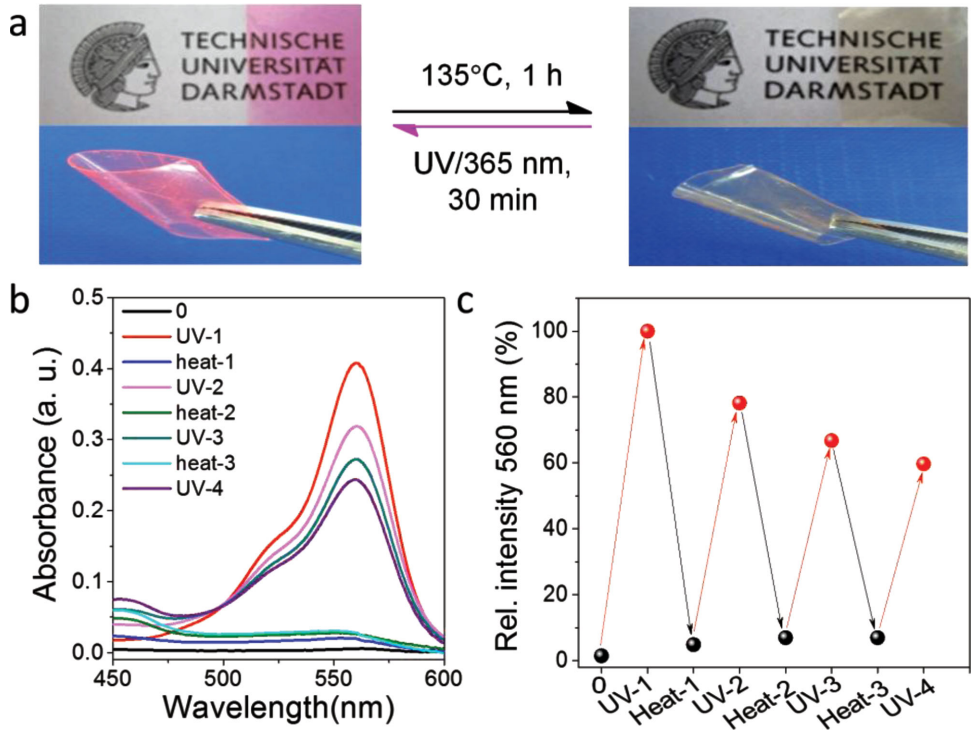

Figure 4. a) Photo images of a transparent nanocomposite film of 43.8 ± 2.8 µm from SS-CNPs and C18-RhB with switchable colors after the UV-illumination at 365 nm and heating at 135 °C; b) UV–vis absorption spectra; and c) Relative absorption intensity of the bands at 560 nm of the nanocomposite films after alternating UV-illumination and heating. The standard deviations were all <5%. The relative intensity of the absorbance bands at 560 nm after the first UV-illumination at 365 nm for 30 min was assigned as 100%.

decreased due to the photofatigue (the loss of performance in photoisomerization).[20] The responsive properties are derived from rhodamine spiroamide, which is structurally present as ring-closed and ring-open form depending on external stimuli, e.g., UV-illumination, heating or pH values.[21]

The homogeneous distribution of C_{18}–RhB within the SS-CNPs films is ascribed to the presence of the hydrophobic stearoyl groups, which can strongly interact with the surface-attached stearoyl groups at SS-CNPs and cannot be extracted by THF (Figure S9, Supporting Information). In comparison, SS-CNPs and rhodamine (RhB) at a ratio of 95/5 (w/w) did not form self-standing films, but only resulted in small cracks during the drying process. RhB could be simply removed by THF (Figure S9, Supporting Information). Thus, RhB could not be effectively encapsulated due to the lack of the interactions between SS-CNPs and RhB.

2.3. Responsive Shape-Memory Property

The SS-CNPs films further showed a responsive shape-memory behavior. A strip of SS-CNPs film could be transformed into a stable spiral shape after heating at 80 °C for 30 min or soaking in THF for 2 s (**Figure 5**). An external force has to be applied to fix the shape. After cooling down or evaporation of THF, SS-CNPs films in spiral shape were obtained. The original flat form of the films was recovered under THF atmosphere after an exposure for only 12 s (Figure 5 and Movie S1, Supporting Information). In comparison, the initial flat form of the coiled SS-CNPs film could not be restored after the treatment at 80 °C for long time, e.g., 24 h. An external force such as pressing or straining was required during the heating and cooling down, in order to recover the form of the films back to their initial shape (Figure 5).[22] Due to the strong interaction between stearoyl groups and THF, THF can destruct crystalline regions formed by stearoyl groups at the surface of SS-CNPs by binding to them and separate them (**Scheme 2**). The binding

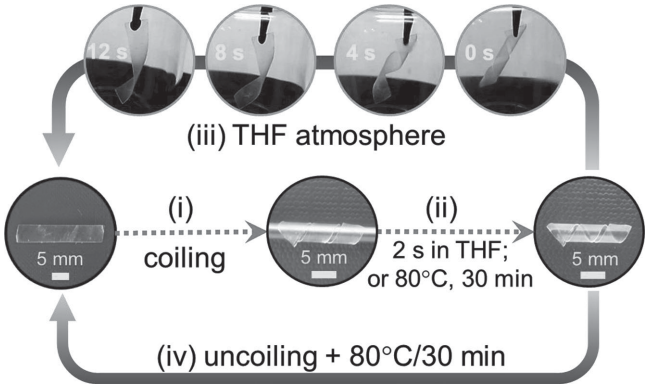

Figure 5. Schematic demonstration of the responsive shape-memory behavior of the SS-CNPs film strips: i) A strip was coiled around a cylinder to give a spiral shape; ii) The precoiled strip was treated via soaking in THF or heating at 80 °C to yield a stable spiral shape; iii) The strip with the spiral shape was placed above hot THF 50 °C) within a beaker to check the solvent-responsive shape-memory property; iv) The film with a spiral shape was uncoiled with an external force and heating at 80 °C for 30 min.

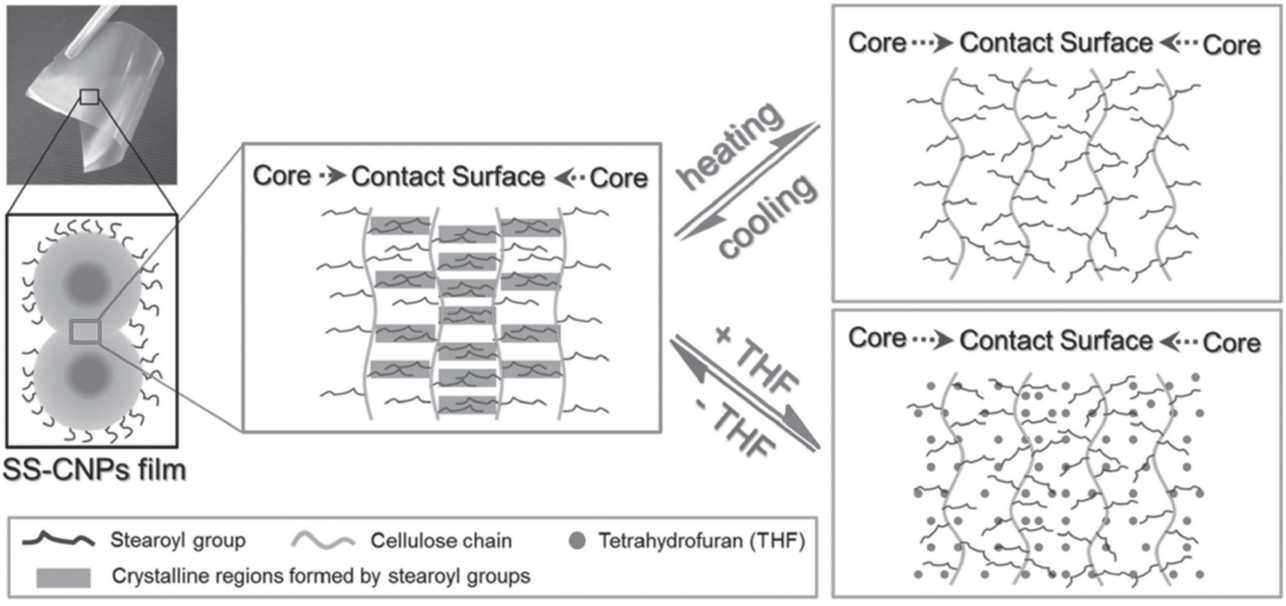

Scheme 2. Schematic illustration for the reversible construction and destruction of crystalline regions formed by stearoyl groups inside the SS-CNPs films via heating or absorbing THF.

between stearoyl groups and THF molecules releases the inner stress that was established during the formation of the spiral shape, leading to the recovery of the original shape. However, the heating cannot separate the stearoyl groups, although the crystalline regions formed by stearoyl groups represent a decrystallization temperature around 53 °C according to DSC measurement (Figure S10, Supporting Information).[23] This responsive shape-memory property allows the SS-CNPs films for the construction of various actuators of sensors.[24] Due to the sustainable and biocompatible character of cellulose, they are promising for versatile biomedical applications.

3. Conclusion

In summary, an efficient method for the preparation of novel surface-stearoylated cellulose nanoparticles (SS-CNPs) showing an average size of 115 ± 0.5 nm and an average DS of 1.33 was reported. SS-CNPs were obtained after a one-step esterification of cellulose fibers using stearoyl chloride under heterogeneous reaction conditions. SS-CNPs contained crystalline cellulose core according to solid-state CP/MAS ^{13}C NMR spectroscopy. SS-CNPs showed excellent dispersibility in nonpolar solvents, such as THF, dichloromethane, and cyclohexane. THF-suspensions of SS-CNPs formed temperature-responsive organogels at low temperature (e.g., 4 °C) or at RT for long time (e.g., 4 d). After solvent-casting, THF-suspension of SS-CNPs, transparent and self-standing hydrophobic films with reversibly solvent-responsive surface wettability and responsive shape-memory property were obtained. THF and acetone exhibited surface-smoothing and roughing agent, respectively. The coiled SS-CNPs films showed nearly full recovery of the original flat shape after only 12 s exposure to THF atmosphere. Moreover, the films from SS-CNPs showed excellent interaction with nonpolar compounds, e.g., (2-stearoylaminoethyl) rhodamine B (C_{18}–RhB) could be encapsulated inside the films. The films containing C_{18}–RhB were endowed with UV- and temperature-responsive optical colors and correlated fluorescence. At the same time, the transparency of films was maintained. Thus, these novel nanoparticles based on sustainable cellulose exhibit various advantageous functions and they provide a new platform for the construction of functional materials in diverse forms, such as organogels and films.

4. Experimental Section

Materials: Microcrystalline cellulose (MCC) with granule size of 50 µm and stearoyl chloride (90%) were bought from Sigma-Aldrich (Steinheim, Germany). Deionized water (DI) was used in all experiments. Other chemicals are all of analytical grade and used as received.

Synthesis and Purification of Surface-Stearoylated Cellulose Nanoparticles (SS-CNPs): Surface-stearoylated cellulose nanoparticles (SS-CNPs) were prepared according to the synthesis reported before with a few modifications.[23b,25] In a typical case, cellulose (1 g) was washed with methanol to remove traces of moisture, before it was suspended in pyridine (30 mL). The mixture was heated up to 100 °C and stearoyl chloride (6.91 mL, 3 mol stearoyl chloride per mol anhydroglucose units of cellulose) was dropped to the hot cellulose suspension under stirring, while the system was purged with nitrogen. After 1 h stirring at 100 °C, the hot reaction mixture was poured into 200 mL ethanol. The precipitate was separated by centrifugation. Thereafter, the product was repeatedly swollen in dichloromethane and precipitated in 5 volumes ethanol, before the product was thoroughly rinsed with ethanol and dried. In order to prepare the SS-CNPs, the powdery product was dispersed in THF and treated with ultrasonication for 1 h at 0 °C. Then, the suspension was centrifuged for 20 min at 12 000 rpm at 4 °C for 3× to remove soluble components. After the centrifugation, the supernatant was removed and the solid was dispersed in THF again, which was centrifuged for 20 min at 3000 rpm at 20 °C to remove the microscaled segments. Finally, the purified product was dispersed in THF for further use. Yield of SS-CNPs: 47.3%. Degree of substitution (DS): 1.33 according to elemental analysis.

Formation of Organogel: The suspensions containing 100 mg SS-CNPs homogenously dispersed in the 5 mL THF were stored in a refrigerator at 4 °C for 2 h or stored at room temperature (RT) for 4 d, leading to organogels.

Fabrication of Self-Standing Films with Switchable Surface Wettability and Responsively Shape-Memory Property: Transparent hydrophobic films were obtained after the deposition of homogeneous THF-suspensions of SS-CNPs on Teflon dish using solvent-casting technique. Then, the original films (referred as F1-THF-1) were dipped into THF solvent for 10 s and immediately transferred into acetone for 10 s, leading to F1-AT-1. The F1-AT-1 films were dipped again in THF for 10 s and dried as F1-THF-2. This process was iterated, and the treated films were referred as F1-AT-2, F1-THF-3, F1-AT-3 ... F1-AT/THF-*n* in sequence (Figure 3a).

Fabrication of Transparent Nanocomposite Films with Switchable Colors: For the fabrication of transparent nanocomposite films with switchable colors, (2-stearoylaminoethyl) rhodamine B (C_{18}–RhB) was dissolved in THF-suspension of SS-CNPs at the ratio of C_{18}–RhB:SS-CNPs = 5/95 (w/w). Transparent nanocomposite films were obtained by decanting the suspension into a Teflon dish and further evaporation of THF at ambient temperature.

Elemental Analysis: The contents of carbon, hydrogen, and nitrogen were determined with an Elemental Analyser vario EL III CHN (Elementar, Hanau, Germany). The total degree of substitution (DS) ascribed to stearoyl groups was calculated according to the ref.[12].

FTIR Spectroscopy: FTIR spectroscopy was conducted on Spectrum One FTIR Spectrometer (PerkinElmer, USA) at RT between 4000 and 600 cm^{-1} with a resolution of 4 cm^{-1}. The samples were measured twice per 32 scans and average spectra were generated for each sample.

Solid-State CP/MAS ^{13}C NMR Spectroscopy: Solid-state CP/MAS ^{13}C NMR spectroscopy was performed on a Bruker Avance III HD spectrometer (Bruker Biospin, Ettlingen, Germany) at RT with a ^{13}C frequency of 75.47 MHz, 8 kHz spinning speed, 3 ms of contact time and ^{1}H decoupling of 20 tppm.

Scanning Electron Microscopy (SEM): SEM images were obtained with a Philips XL30 FEG high-resolution scanning electron microscope (HR-SEM) (FEI Deutschland GmbH, Frankfurt/Main, Germany). A layer from platinum/palladium of 10 nm was coated on the surface of samples before SEM measurements.

Dynamic Light Scattering (DLS): The DLS measurement was performed on a Zetasizer Nano ZS (Malvern Instruments Ltd., UK) using 5 mW laser with the incident beam of 633 nm (He–Ne laser). For the particle size measurement, the SS-CNPs suspensions were diluted with THF to a concentration of 1 mg mL^{-1}. 1 mL of each suspension in a quartz cuvette (Type 3 from Starna GmbH, Pfungstadt, Germany) was used for the size measurement. The Z-average diameter of SS-CNPs was measured 3× with 10 runs and 10 s per run.

Atomic Force Microscopy (AFM): An MFP-3D system (Asylum Research, Santa Barbara, USA) was used for AFM imaging in noncontact mode using cantilevers with resonance frequencies of approximately 150 kHz and a nominal force constant of 5 N m^{-1} (BudgetSensors, Innnovative Solutions Bulgaria Ltd., Sofia, Bulgaria) at a scan speed of 10 µm s^{-1}. The programs IGOR Pro 6.22A (WaveMetrics Inc., Lake Portland, USA) was used to guide the AFM measurements and Gwyddion (Free Software Foundation, Inc., Boston, USA) for the analysis of AFM images, respectively.

Rheological Experiments: Rheological measurements were performed in a Thermo Scientific HAAKE MARS III Rotational Rheometer with parallel plate geometry ($\phi = 25$ mm). The experiments were performed at 25 and 4 °C in a closed chamber. To minimize the solvent evaporation, THF-saturated tissues were placed in the chamber around the samples. Frequency sweep measurements in the frequency range of 1–100 rad s^{-1} with a distance of 0.3 mm between the plates at a strain (γ) of 0.05% were performed, in order to ensure the measurements in the linear viscoelastic regime (which has been determined by dynamic strain sweep measurements).

UV–Vis Measurements: UV–vis measurements of the transparent films and SS-CNPs suspensions in different solvents were carried out on Varian Cary 50 UV–vis Spectrophotometer (Agilent Technologies Deutschland GmbH, Böblingen, Germany) between the wavelengths of 200 and 900 nm at RT.

Static Contact Angles: Static contact angles of 4 µL water drops on film surfaces were measured on Contact Angle System OCA 15EC (dataphysics, Filderstadt, Germany) under controlled conditions at 23 ± 2 °C and a moisture of 50 ± 1%.

Supporting Information

Supporting Information is available from the Wiley Online Library or from the author.

Acknowledgements

Authors thank the Hessian excellence initiative LOEWE—research cluster SOFT CONTROL for the financial support. K.Z. and Y.W. thank Prof. Markus Biesalski for the kind support. Y.W. thanks China Scholarship Council (CSC) for the financial support.

Received: September 5, 2014
Published online: January 22, 2015

[1] a) D. Klemm, F. Kramer, S. Moritz, T. Lindstrom, M. Ankerfors, D. Gray, A. Dorris, *Angew. Chem Int. Ed.* **2011**, *50*, 5438; b) Y. Habibi, L. A. Lucia, O. J. Rojas, *Chem. Rev.* **2010**, *110*, 3479.

[2] a) E. Lam, K. B. Male, J. H. Chong, A. C. Leung, J. H. Luong, *Trends Biotechnol* **2012**, *30*, 283; b) R. J. Moon, A. Martini, J. Nairn, J. Simonsen, J. Youngblood, *Chem. Soc. Rev.* **2011**, *40*, 3941; c) S. J. Eichhorn, *Soft Matter* **2011**, *7*, 303; d) A. Walther, J. V. Timonen, I. Diez, A. Laukkanen, O. Ikkala, *Adv. Mater.* **2011**, *23*, 2924; e) R. T. Olsson, M. A. Azizi Samir, G. Salazar-Alvarez, L. Belova, V. Strom, L. A. Berglund, O. Ikkala, J. Nogues, U. W. Gedde, *Nat. Nanotechnol.* **2010**, *5*, 584.

[3] a) C. Olivier, C. Moreau, P. Bertoncini, H. Bizot, O. Chauvet, B. Cathala, *Langmuir* **2012**, *28*, 12463; b) K. L. Spence, R. A. Venditti, Y. Habibi, O. J. Rojas, J. J. Pawlak, *Bioresour. Technol.* **2010**, *101*, 5961.

[4] a) S. Fujisawa, T. Ikeuchi, M. Takeuchi, T. Saito, A. Isogai, *Biomacromolecules* **2012**, *13*, 2188; b) F. Khelifa, Y. Habibi, P. Leclere, P. Dubois, *Nanoscale* **2013**, *5*, 1082; c) C. C. Y. Cheung, M. Giese, J. A. Kelly, W. Y. Hamad, M. J. MacLachlan, *ACS Macro Lett.* **2013**, *2*, 1016; d) J. R. Capadona, O. Van Den Berg, L. A. Capadona, M. Schroeter, S. J. Rowan, D. J. Tyler, C. Weder, *Nat. Nanotechnol.* **2007**, *2*, 765; e) J. R. Capadona, K. Shanmuganathan, D. J. Tyler, S. J. Rowan, C. Weder, *Science* **2008**, *319*, 1370.

[5] S. Fujisawa, T. Saito, S. Kimura, T. Iwata, A. Isogai, *Biomacromolecules* **2013**, *14*, 1541.

[6] a) S. Fujisawa, Y. Okita, T. Saito, E. Togawa, A. Isogai, *Cellulose* **2011**, *18*, 1191; b) K. H. Kan, J. Li, K. Wijesekera, E. D. Cranston, *Biomacromolecules* **2013**, *14*, 3130; c) Y. Habibi, A.-L. Goffin, N. Schiltz, E. Duquesne, P. Dubois, A. Dufresne, *J. Mater. Chem.* **2008**, *18*, 5002; d) G. Siqueira, J. Bras, A. Dufresne, *Biomacromolecules* **2009**, *10*, 425.

[7] a) J. J. Blaker, K.-Y. Lee, X. Li, A. Menner, A. Bismarck, *Green Chem.* **2009**, *11*, 1321; b) R. K. Johnson, A. Zink-Sharp, W. G. Glasser, *Cellulose* **2011**, *18*, 1599.

[8] S. Vuoti, R. Talja, L.-S. Johansson, H. Heikkinen, T. Tammelin, *Cellulose* **2013**, *20*, 2359.

[9] a) M. Fumagalli, F. Sanchez, S. M. Boisseau, L. Heux, *Soft Matter* **2013**, *9*, 11309; b) M. Fumagalli, D. Ouhab, S. M. Boisseau, L. Heux, *Biomacromolecules* **2013**, *14*, 3246; c) S. Berlioz, S. Molina-

Boisseau, Y. Nishiyama, L. Heux, *Biomacromolecules* **2009**, *10*, 2144.
[10] G. Siqueira, J. Bras, A. Dufresne, *Langmuir* **2010**, *26*, 402.
[11] W. Shang, J. Huang, H. Luo, P. R. Chang, J. Feng, G. Xie, *Cellulose* **2012**, *20*, 179.
[12] C. Vaca-Garcia, M. E. Borredon, A. Gaseta, *Cellulose* **2001**, *8*, 225.
[13] a) P. Jandura, B. V. Kokta, B. Riedl, *J. Appl. Polym. Sci.* **2000**, *78*, 1354; b) L. Crepy, V. Miri, N. Joly, P. Martin, J. M. Lefebvre, *Carbohydr. Polym.* **2011**, *83*, 1812.
[14] P. S. Belton, S. F. Tanner, N. Cartier, H. Chanzy, *Macromolecules* **1989**, *22*, 1615.
[15] A. Geissler, E. Bonaccurso, L.-O. Heim, T. Heinze, K. Zhang, *J. Phys. Chem. C* **2014**, *118*, 2408.
[16] Z. L. Chu, Y. J. Feng, *Chem. Commun.* **2011**, *47*, 7191.
[17] a) M. Osterberg, J. Vartiainen, J. Lucenius, U. Hippi, J. Seppala, R. Serimaa, J. Laine, *ACS Appl. Mater. Interfaces* **2013**, *5*, 4640; b) H. L. Zhu, Z. Q. Fang, C. Preston, Y. Y. Li, L. B. Hu, *Energy Environ. Sci.* **2014**, *7*, 269.
[18] S. Zhang, N. Ali, *Nanocomposite Thin Films and Coatings: Processing, Properties and Performance*, Imperial College Press, London **2007**.
[19] a) V. N. Belov, C. A. Wurm, V. P. Boyarskiy, S. Jakobs, S. W. Hell, *Angew. Chem Int. Ed.* **2010**, *49*, 3520; b) V. N. Belov, M. L. Bossi, J. Folling, V. P. Boyarskiy, S. W. Hell, *Chem. Eur. J.* **2009**, *15*, 10762.
[20] R. Tong, H. D. Hemmati, R. Langer, D. S. Kohane, *J. Am. Chem. Soc.* **2012**, *134*, 8848.
[21] a) M. Beija, C. A. M. Afonso, J. M. G. Martinho, *Chem. Soc. Rev.* **2009**, *38*, 2410; b) Y. Shiraishi, R. Miyamoto, X. Zhang, T. Hirai, *Org. Lett.* **2007**, *9*, 3921.
[22] a) K. Li, J. Song, M. Xu, S. Kuga, L. Zhang, J. Cai, *ACS Appl. Mater. Interfaces* **2014**, *6*, 7204; b) B. T. Michal, C. A. Jaye, E. J. Spencer, S. J. Rowan, *ACS Macro Lett.* **2013**, *2*, 694.
[23] a) J. E. Sealey, G. Samaranayake, J. G. Todd, W. G. Glasser, *J. Polym. Sci. Part B: Polym. Phys.* **1996**, *34*, 1613; b) C. Vaca-Garcia, G. Gozzelino, W. G. Glasser, M. E. Borredon, *J. Polym. Sci Part B: Polym. Phys.* **2003**, *41*, 281.
[24] a) J. R. Kumpfer, S. J. Rowan, *J. Am. Chem. Soc.* **2011**, *133*, 12866; b) K.-U. Jeong, J.-H. Jang, D.-Y. Kim, C. Nah, J. H. Lee, M.-H. Lee, H.-J. Sun, C.-L. Wang, S. Z. D. Cheng, E. L. Thomas, *J. Mater. Chem.* **2011**, *21*, 6824; c) M. Ji, N. Jiang, J. Chang, J. Sun, *Adv. Funct. Mater.* **2014**, *24*, 5412.
[25] A. Geissler, L. Chen, K. Zhang, E. Bonaccurso, M. Biesalski, *Chem. Commun.* **2013**, *49*, 4962.